J Mater Sci (2008) 43:4573–4582
DOI 10.1007/s10853-008-2686-y

Structural and textural characterization of a novel spatially coherent crystalline nanocomposite obtained from a melt of KBr, RbCl, RbBr, KI, RbI, and KCl salts

A. E. Cordero-Borboa · R. R. Mijangos · L. Flores-Morales

Received: 6 September 2007 / Accepted: 29 April 2008 / Published online: 13 May 2008

Abstract Large crystal bulks, grown by the Czochralski technique from a melt prepared by mixing equal molar fractions of KBr, RbCl, RbBr, KI, RbI, and KCl salts, are characterized by X-ray diffractometry and atomic force microscopy. The bulk material consists of a highly textured aggregation of crystallites of two different face-centered-cubic-solid solutions with unit-cell sizes of 7.247 ± 0.001 and 6.536 ± 0.005 Å, in molar fractions of 1/3 and 2/3, respectively. These solutions are discussed to be the binary KI(34.4%):RbI(65.6%) and the quaternary KBr(42.7%):RbCl(33.2%):RbBr(8.1%)KCl(16.0%) mixed phases, respectively. Most of the crystallites, no matter the phase they belong to, are spatially coherent to each other. Freshly cleaved {100}-faces show surface domains, surrounded by canyons, and surface steps. These domains are plenty of knolls (1.8 ± 0.1 knolls/μm^2) with a corresponding average knoll-profile full-width-at-half-maximum-value of 0.054 ± 0.003 μm, suggesting that the material is formed by a mass of individual nanometric grains. Micrometric particles, showing defined crystallographic habits, are immersed within the growths so that they keep in common with the growth matrix important crystallographic directions. The expected consequences of the observed texture on the physical properties of the material, as well as the structural origin of both the observed surface steps and the whitish visual appearance of the growths, are discussed.

A. E. Cordero-Borboa (✉)
Departamento de Materia Condensada, Instituto de Física, Universidad Nacional Autónoma de México, A.P. 20-364, Mexico DF 01000, Mexico
e-mail: cordero@fisica.unam.mx

R. R. Mijangos
Centro de Investigación en Física, Universidad de Sonora, A.P. 5–88, Hermosillo, Sonora 83190, Mexico
e-mail: mijangos@cajeme.cifus.uson.mx

L. Flores-Morales
Departamento de Física, Facultad de Ciencias, Universidad Nacional Autónoma de México, Mexico DF 04510, Mexico
e-mail: lfm@fciencias.unam.mx

Introduction

This paper reports the structural and textural characterizations of a novel crystalline-mixed alkali-halide composite material that was obtained by pulling techniques from a melt previously prepared by mixing together equal molar fractions of pure KBr, RbCl, RbBr, KI, RbI, and KCl salts. These salts have been the subjects of pioneering X-ray diffraction works. The Braggs used KBr, KI, and KCl, aside of halite, to carry out the first-ever X-ray diffraction crystal structure determinations [1, 2], and, soon after that, these salts were studied by Glocker [3, 4], and Hull [5], by means of Laue photography and powder X-ray diffractometry (XRD), respectively. RbBr, RbCl, and RbI were studied around 1921 by Davey [6], Wyckoff [7] and Posnak and Wyckoff [8] by means of single-crystal and powder XRD. The structure of a mixed alkali-halide crystal was characterized for the first time by Vegard and Schjelderup as early as 1917 [9, 10], by working on the binary mixed KCl:KBr system. This system resulted to be a face-centered-cubic (fcc) substitutional solid solution whose lattice unit-cell size may be computed as the weighed sum of the KCl- and KBr-unit-cell sizes, being the weights in this sum the relative concentrations of the Cl^- and Br^- ions, respectively, in the KCl:KBr solid solution (a statement that is known now a days as the Vegard's rule). Since then, other binary mixed alkali-halide systems have been

studied from the structural point of view, and an excellent compilation of the results obtained from these studies, including some solid-solution solubility properties, has been written by Kitaigorodsky [11]. An empirical corollary obtained from such studies is, in particular, that a complete substitutional binary alkali-halide solid-solution series may in principle be formed from two alkali-halide salts whenever the relative difference in unit-cell-size between these salts is less than about 10% [11, 12]. This corollary, whose structural origin rests on the fact that the crystal lattice distortion associated [13, 14] to ions of different atomic elements replacing to each other during the formation of the solid solution may be so large that the formation of a stable mixed lattice is forbidden, is currently used as a criterion to discern whether, in principle, a solid solution is expected or not to form from a melt of two certain salts. From the 15 different binary combinations that may be obtained by shuffling in pairs the six alkali halides used, as precursor salts, in the present work, only 11 satisfy the 10%-unit-cell-size-difference criterion. From these 11 combinations (shown in Table 1 together with the corresponding solid-solution unit-cell-size-range limits and relative differences between these limits) only 9 (the exceptions are KI:RbCl and KI:RbBr) have been currently obtained [11, 16, 17] in the laboratory as complete substitutional alkali-halide solid-solution series. Even that mixed crystals of NaCl–KCl [18], NaCl–KCl–KBr [19] and NaCl–NaBr–NaI [20] as well as multiphased mixed crystals from the mixtures of NaBr–KCl [21], NaCl–KCl–KBr [22], and NaCl–KBr–KI [23] have been obtained, crystalline materials grown from melts prepared by mixing together more than two of the six different alkali-halide salts used as precursor salts in the present work have been scarcely reported to be either obtained or studied. Few years ago, large crystal bulks were obtained from melts that were previously prepared by mixing together equal molar parts of three (KBr, RbCl, and KCl) [24] and four (KBr, RbCl, RbBr, and KCl) [25] different fcc-alkali halides, and then characterized by XRD [24, 26]. The structure of the material forming these bulks might be described as that of a ternary (KBr:RbCl:KCl) and a quaternary (KBr:RbCl:RbBr:KCl), respectively, fcc-substitutional solid solution. Another important result from such works was that the measured unit-cell size for these solutions was found to agree with the unit-cell-size value predicted by using a generalized Vegard's rule for ternary and quaternary, respectively, mixed systems. Few years ago also, crystals obtained by the Czrochalski technique from ternary melts (prepared by mixing together KCl, KBr, and KI salts in different relative concentrations) and then characterized by using powder XRD, among other techniques, have been reported [27] to be multiphased systems formed by an aggregate of two separate fcc-phases of which one nearly corresponds to KI and the other nearly corresponds to a KCl:KBr mixed system. Recently, large crystal bulks obtained from melts that were previously prepared by mixing together equal molar parts of five different fcc-alkali halides (KBr, RbCl, RbBr, KI, and RbI) have been studied [28] by XRD, Laue photography, and field-emission high-resolution electron microscopy. According to this study, the material forming these bulks resulted to be a composite material consisting of an aggregation of nanocrystallites (ranging in size from 5 to 60 nm) of three different phases. From these phases, one was identified as an unmixed phase (RbBr), another one was identified as a binary mixed phase [KI(39%):RbI(61%)], and the third one was discussed to be a ternary mixed phase [KBr(47%):RbCl(39%):RbBr(14%)]. A most striking result from such studies was that the crystallites forming the composite, no matter the particular phase they belong to, were found to have a strong preferred orientation in the space (with a maximum deviation of about 2.7° from the common spatial direction). Even when this last result makes the studied spatially coherent mixed alkali-halide composite an important material from the point of view of crystal engineering and design (as discussed elsewhere), no other spatially coherent mixed alkali-halide composite has been reported to be studied as far as the authors are aware.

In the present work, XRD and atomic force microscopy (AFM) studies carried out on large crystal bulks of another spatially coherent mixed alkali-halide composite, which was previously obtained from a melt of six different alkali-halide salts (KBr, RbCl, RbBr, KI, RbI, and KCl), are reported.

Table 1 Solid-solution unit-cell-size range limits, and their corresponding differences, for the binary combinations that may be obtained, satisfying the 10%-unit-cell-size difference criterion, by shuffling in pairs the KBr, RbCl, RbBr, KI, RbI, and KCl salts

Binary combination	Solid-solution unit-cell-size range limits[a] (Å)		Solid-solution unit-cell-size range limits difference (%)
KBr:KCl	6.6005	6.291	4.9
KBr:KI	6.6005	7.065	7.0
RbCl:RbBr	6.5810	6.889	4.7
RbI:RbBr	7.342	6.889	6.5
KCl:RbCl	6.291	6.5810	4.6
KBr:RbBr	6.6005	6.889	4.4
KI:RbI	7.065	7.342	4.0
KCl:RbBr	6.2917	6.889	8.7
KI:RbCl	7.065	6.5810	6.9
KI:RbBr	7.065	6.889	2.5
RbCl:KBr	6.5810	6.6005	0.3

[a] Reference [15]

Experimental details

Large crystal bulks were obtained (Fig. 1) by the Czochralski technique [29] from a melt prepared by mixing together equal molar fractions of pure KBr, RbCl, RbBr, KI, RbI, and KCl salts. From these salts, the potassium halides were purchased, reagent-grade labeled, from J.T. Baker Co. with essay purities of 101.1, 99.5, and 99.9%, respectively. According to the corresponding labels, the superior limits of the dominant impurities in these reagents were the following: for KBr, 0.001% of BrO_3, 0.001% of Cl, 0.001% of I, 0.002% of nitrogen compounds, 0.003% of sulfates, 0.002% of Ba, and 0.02% of Na; for KI, 0.01% of Cl and Br, 0.001% of nitrogen compounds, 0.005% of phosphates, 0.005% of sulfates, 0.002% of Ba, and 0.003% of Na; and for KCl, 0.01% of Br, 0.001% of Cl and nitrates, 0.002% of I, 0.001% of nitrogen compounds, 0.001% of sulfates, 0.001% of Ba, and 0.002% of Na; while the rubidium halides were purchased from Sigma Aldrich Co. with essay purities of 99.99, 99.7, and 99.9%, respectively. Information about the dominant natural impurities in these halides, with Chemical-Abstract-Service numbers 7791-11-9, 7789-39-1, and 7790-29-6, respectively, was not available. A dry argon atmosphere was maintained inside the growing chamber in order to avoid contamination by molecules and ions in the air like H_2O, O_2, and OH^-. Once grown, the crystal bulks were cooled from freezing temperature to room temperature naturally. The crystal bulks were observed to be transparent near the freezing point and then to become whitish as the crystal bulk temperature approaches the room temperature. After cooling, the bulks were found to be easily exfoliated along their cubic {100}-faces. Along these faces plate-like samples of sizes about $1.0 \times 1.0 \times 0.1$ cm^3 were cleaved off in order to be used as single-plate XRD specimens for textural studies, while some remnant fragments were ground to powder in an agate mortar and then mixed (20% by weight) with powder of silicon, used as an internal standard, in order to get suitable powder XRD-specimens for phase identification and unit-cell-size measurements. For the purposes of textural characterization, phase identification, and unit-cell-size measurement, diffractograms were taken in the range from 5 to 130° in twice the Bragg angle (2θ), using counting times of 1, 4, and 20 s, respectively, per a scanning step of 0.02° (in 2θ) in all the cases. This was done by using a Siemens-D5000 diffractometer equipped with a variable divergence diaphragm, a secondary-arm graphite monochromator, and a Cu-anode X-ray tube (working at operation conditions of 35 kV–25 mA). Plate-like specimens were mounted on the diffractometer so that one of their {100}-faces, resulting from cleavage, coincided with the diffractometer sample-cup main plane. Powder diffractograms were calibrated in 2θ using a calibration curve that was previously built by plotting the difference between the observed and the expected 2θ-positions for the diffraction peaks corresponding to silicon versus 2θ. In these diffractograms, the intensity maxima positions of the observed reflections were measured in 2θ and then used to calculate, by means of the Bragg's law, the corresponding lattice interplanar distances $d_{2\theta}$. These distances were then used to assign a set of reflection *HKL*-indexes, as well as a set of lattice-parameter values a_{HKL}, to each of the two sets of observed reflections. For each of these sets, two values of the corresponding unit-cell size a_0 were estimated. In order to do this, the assigned a_{HKL}-values were plotted against $\cos^2\theta$ and $\cos\theta\ \cot\theta$, then straight lines were fitted to the plotted data, by using the least-square-based Cohen's method [30, 31], and, finally, these lines were extrapolated to 90° in θ. For every phase forming the sample, the two estimated a_0-values were found to be experimentally equal to each other, while the corresponding fitted lines were found to have typical slopes of about 1×10^{-3} and 5×10^{-4} Å, in the $\cos^2\theta$ and $\cos\theta\ \cot\theta$-cases, respectively. Since the relative $d_{2\theta}$-variation is expected [32] to be proportional to $\cos^2\theta$ or $\cos\theta\ \cot\theta$ depending on whether the specimen-surface-displacement error or the flat-specimen-and-transparency error is larger, respectively, such low-slope magnitude values mean that, in our experiment, the first of these two errors was practically eliminated by means of the used silicon-internal-standard calibration, while the second of these errors is comparable in magnitude with the obtained a_0-experimental accuracy. Plate-like specimens for AFM were obtained by exfoliating the crystal growth along the mechanically observed crystallographic ⟨110⟩-directions so that the crystallographic

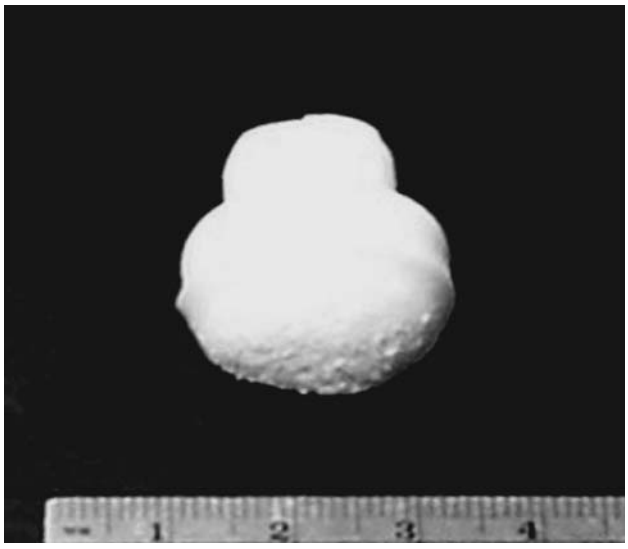

Fig. 1 Photograph of a typical crystal bulk obtained by the Czochralski technique from a melt prepared by mixing equal molar fractions of pure KBr, RbCl, RbBr, KI, RbI, and KCl salts

{100}-faces were exposed. These faces were examined with the help of a Nanosurf EasyScan AFM equipped with a standard Nanosensors silicon probe working in the contact mode with a *Z*-range of about 2.8 μm.

Results

Powder XRD

Figure 2 shows a detail, corresponding to a 2θ-range from 20 to 92°, of a typical powder X-ray diffractogram of a crystal growth obtained from a melt that was previously prepared by mixing equal molar fractions of KBr, RbCl, RbBr, KI, RbI, and KCl salts. In this detail, 21 well-defined Bragg reflections may be observed to appear (1–21 in the figure), aside from the internal-standard-silicon diffraction *HKL*-signals (SiHKL in the figure), making evident that the sample is well crystallized. The standard diffraction line patterns corresponding [15] to the salts used to prepare the mother melt are also shown, for the sake of comparison, in Fig. 2 (◯, ■, ▲, □, ●, and △, respectively). These patterns may be seen in the figure to be unmatched by the observed reflections, suggesting that the structure of the material under characterization is that of a solid-solution system. In order to characterize this system, the observed reflections were measured in 2θ, and, then, from these measurements the corresponding interplanar distances $d_{2\theta}$ were computed by means of the Bragg's law. Then, by using these distances some of the observed reflections (e.g., 1, 2, 4, 6, 7, 9–12, 14, 16–18, and 20 in Fig. 2) were properly indexed on the basis of an fcc-type phase with a unit-cell size a_{0B} of 7.247 ± 0.001 Å (called as phase B from here on in this article). The rest of the observed reflections (e.g., reflections 3, 5, 8, 13, 15, and 19 in Fig. 2) were properly indexed on the basis of an fcc-type phase with a unit-cell size a_{0Q} of 6.536 ± 0.005 Å (called as phase Q from here on in this article). The assigned *HKL*-indexes as well as the measured d_{HKL}-values and relative diffraction intensities I_{HKL} for the observed reflections associated to phases B and Q are shown, for the sake of further comparison, in Tables 2 and 3, respectively.

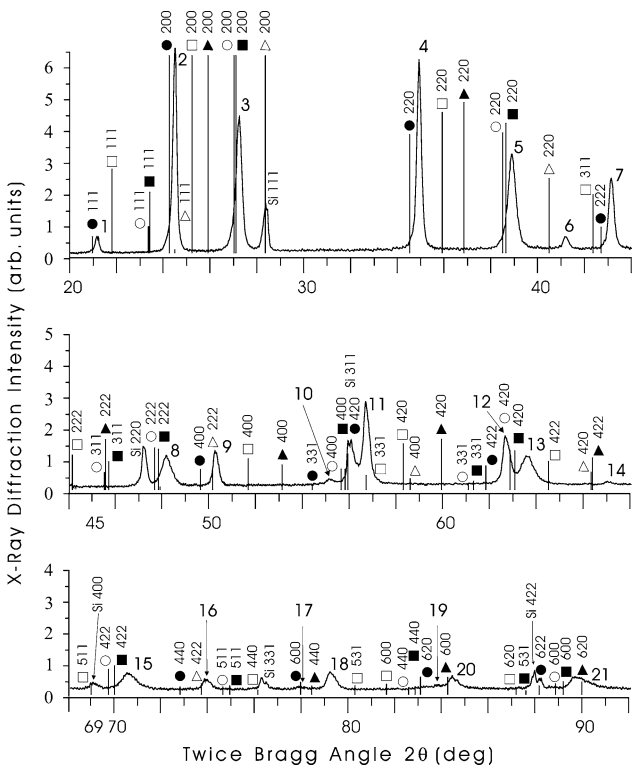

Fig. 2 Detail of a typical powder XRD of the crystal bulk shown in Fig. 1. Twenty-one well-defined reflections (1–21), aside from the reflections corresponding to the internal standard silicon (SiHKL), may be seen to appear from a flat background line. The ICDD-PDF-card lines corresponding to KBr, RbCl, RbBr, KI, RbI, and KCl salts (◯, ■, ▲, □, ●, and △, respectively) are also shown

Comparison of the measured value for a_{0B} with the solid-solution unit-cell-size range limits listed in Table 1 shows that from the 11 different binary mixed systems that may in principle be formed from the alkali halides used as precursor salts, only RbBr:RbI and KI:RbI are compatible in unit-cell size with phase B. It is worth to do mention here that complete substitutional solid-solution series have been already obtained [11] in the laboratory for these two systems. The general theory [33] that for an ionic fcc-crystal the I_{HKL}-values with $H + K + L$ odd are particularly sensitive to the difference in atomic number between the cations and the anions forming the crystal may help to discern whether the system RbBr:RbI is or is not a better candidate than the system KI:RbI to be assigned to phase B. The standard-diffraction-line-pattern I_{111}-values corresponding [15] to RbI, RbBr, and KI, the salts that are involved in the systems RbBr:RbI and KI:RbI, are about 4.5, 0.0, and 13.7, respectively, once normalized to each other by using the empirical method that has been already described in other work [28], while the measured I_{111}-value for phase B is about 10 (as shown in Table 2). Therefore, under the assumption (see section "On the identity of phase B") that phase B is a binary mixed phase, the KI:RbI-system is the best candidate to be assigned to this phase. Since this system is well known [12] to satisfy strictly the Vegard's rule, this rule was then used to calculate, from the measured value for a_{0B}, the relative concentrations of the KI- and RbI-type components in phase B, resulting to be about 0.34 and 0.66, respectively.

Comparison of the measured value for a_{0Q} with the solid-solution unit-cell-size range limits listed in Table 2 shows that from the 11 different binary mixed systems that may in principle be formed from the alkali halides used as precursor salts, only KBr:KCl, KCl:RbCl, and KCl:RbBr

Table 2 Measured diffraction data and assigned reflection indexes for phase B

Reflection number[a]	Measured interplanar spacing (Å)	Measured relative intensity I_R (%)	Assigned reflection indexes *HKL*	Corresponding lattice parameter a_{HKL} (Å)
1	4.19 ± (0.01, 0.02)	10	111	7.26 ± (0.02, 0.04)
2	3.63 ± (0.01, 0.02)	100	200	7.26 ± (0.03, 0.04)
4	2.562 ± (0.008, 0.012)	92	220	7.25 ± (0.02, 0.03)
6	2.185 ± (0.006, 0.009)	9	311	7.25 ± (0.02, 0.03)
7	2.091 ± (0.006, 0.008)	37	222	7.24 ± (0.02, 0.03)
9	1.811 ± (0.005, 0.007)	20	400	7.25 ± (0.02, 0.03)
10	1.662 ± (0.004, 0.005)	6	331	7.25 ± (0.02, 0.02)
11	1.620 ± (0.003, 0.004)	43	420	7.25 ± (0.01, 0.02)
12	1.479 ± (0.003, 0.003)	27	422	7.25 ± (0.01, 0.01)
14	1.392 ± (0.002, 0.003)	5	333	7.24 ± (0.01, 0.01)
16	1.281 ± (0.002, 0.002)	8	440	7.25 ± (0.01, 0.01)
17	1.225 ± (0.001, 0.002)	4	531	7.247 ± (0.007, 0.009)
18	1.208 ± (0.001, 0.001)	12	442, 600	7.247 ± (0.008, 0.010)
20	1.146 ± (0.001, 0.001)	510	620	7.247 ± (0.007, 0.008)
25	0.968 ± (0.001, 0.001)	6	642	7.246 ± (0.007, 0.009)
28	0.8788 ± (0.0005, 0.0006)	6	644	7.247 ± (0.004, 0.005)

[a] In Fig. 2

Table 3 Measured diffraction data and assigned reflection indexes for phase Q

Reflection number[a]	Measured interplanar spacing *d* (Å)	Measured relative intensity I_R (%)	Assigned reflection indexes *HKL*	Corresponding lattice parameter a_{HKL} (Å)
3	3.27 ± (0.01, 0.02)	100	200	6.54 ± (0.03, 0.04)
5	2.309 ± (0.009, 0.013)	76	220	6.53 ± (0.03, 0.04)
8	1.884 ± (0.007, 0.009)	27	222	6.52 ± (0.02, 0.03)
13	1.460 ± (0.004, 0.004)	26	420	6.53 ± (0.02, 0.02)
15	1.333 ± (0.004, 0.004)	17	422	6.53 ± (0.02, 0.02)
22	1.033 ± (0.003, 0.003)	9	620	6.53 ± (0.02, 0.02)
24	0.984 ± (0.002, 0.001)	7	622	6.53 ± (0.01, 0.01)
26	0.9436 ± (0.0007, 0.0007)	6	444	6.538 ± (0.005, 0.005)
27	0.905 ± (0.001, 0.001)	7	640	6.53 ± (0.01, 0.01)

[a] In Fig. 2

are compatible in unit-cell size with phase Q. The data shown in Table 1 are also useful to search for the ternary and quaternary combinations that may be obtained by shuffling in triads and tetrads, respectively, the alkali halides used as precursor salts, so that every alkali halide in the combination satisfies the empirical 10% unit-cell-size difference criterion with the others. From such combinations, only the ternary KBr:KCl:RbCl-, KBr:KCl:RbBr-, and RbCl:KCl:RbBr-ones, as well as the quaternary KBr:RbCl:RbBr:KCl-one, are compatible in unit-cell size with phase Q. These considerations show that, no matter whether phase Q is thought to exist as a binary, ternary, or quaternary solid-solution, no I^- ions, i.e., only K^+-, Rb^+-, Cl^-, and Br^- -ions, are expected to form part of this phase. The probable identity and composition of phase Q are discussed in section "On the identity of phase Q."

Crystal-plate XRD

Figure 3 shows a typical X-ray diffractogram of a plate-like sample that was previously mounted on the diffractometer so that one of the extended crystallographic {100}-faces coincided with the sample-cup main plane. This diffractogram consists of the 111, 200, 220, 311, and 222-reflections from phase B (B111, B200, B220, B311, and B222, respectively, in the figure), and the 200, 220, and 222-reflections from phase Q (Q200, Q220, and Q222, respectively, in the figure). These reflections were compared in relative diffraction intensity with the corresponding powder *HKL*-reflections. In order to do this, the measured powder I_{HKL}-data sets, as listed in Tables 2 and 3, were previously normalized to the corresponding observed single-plate I_{HKL}-data sets. For the sake of easy

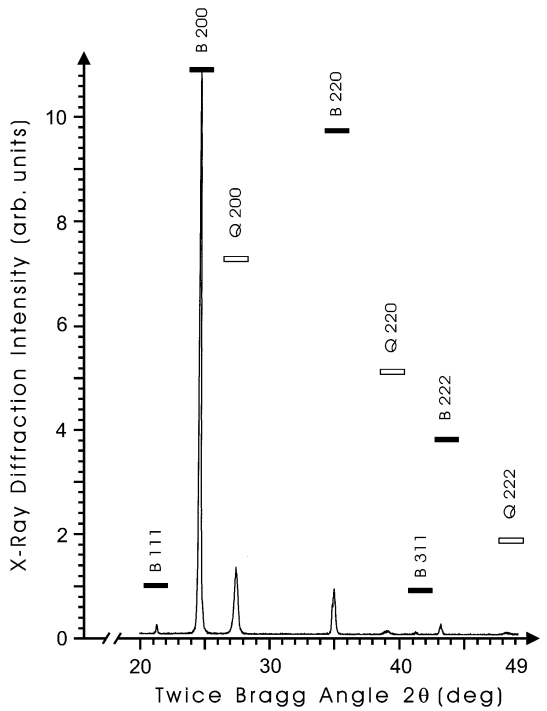

Fig. 3 Typical XRD of a plate-like sample that was previously mounted on the diffractometer so that one of the extended crystallographic {100}-faces coincided with the sample-cup main plane. This diffractogram consists of the 111, 200, 220, 311, and 222-reflections from phase B (B111, B200, B220, B311, and B222, respectively), and the 200, 220, and 222-reflections from phase Q (Q200, Q220, and Q222, respectively). The corresponding normalized powder diffraction intensities for phases B and Q are also indicated (full- and open-short horizontal bars, respectively)

comparison, the normalized powder diffraction intensities corresponding to phases B and Q are indicated in Fig. 3 by using full and open short horizontal bars, respectively. This figure shows that every observed *HKL*-reflection, other than the 200-reflections, has drastically lower relative diffraction intensity than the corresponding powder *HKL*-reflection. Since this experimental situation was observed to happen whatever the mechanically observed crystallographic ⟨100⟩-direction of the crystal growth was chosen to be aligned along the perpendicular to the diffractometer-sample-cup main plane, the individual crystallites forming the growth, no matter the particular phase they belong to, may be inferred to be preferentially oriented in the space in such a way that their individual crystallographic ⟨100⟩-directions lie preferentially along the mechanically observed crystallographic ⟨100⟩-directions of the crystal bulk. The possibility of tailoring as needed the crystallite-lattice anisotropy-depending properties of the studied material, by tuning only either the relative amounts of crystallites of the different phases forming the composite or the composition of these phases, or both, is discussed in section "On the consequences of the observed crystallographic texture on the physical properties."

Atomic force microscopy

Figure 4a shows a typical AFM image of a freshly cleaved {100}-face that was obtained by exfoliating a crystal growth along one of the mechanically observed crystallographic ⟨110⟩-directions (indicated by a heavy dashed line in the figure). The presence, in this image, of some micrometric protuberances (e.g., P1–P4) and cavities (e.g., V1–V4), as well as some straight surface steps (e.g., S1–S6) showing wasted-away step edges, makes evident the fact that the material under study has an inhomogeneous mechanical response to cleavage. The observed protuberances were found to display a morphology consisting of plane faces, indicating [34] that these protuberances have crystallographic habits. The presence of this particular morphology suggests that the observed protuberances are particles of spatially coherent crystalline matter immersed within the spatially coherent composite matrix. The observed habits were found to correspond with some cubic crystallographic forms like the cubo-octahedron and the octahedron. These findings may be illustrated with the help of Fig. 4b showing, as enlarged details of Fig. 4a, the protuberances P1 and P3 (left-bottom and left-top, respectively) together with sketches of a cubo-octahedron, as viewed along a ⟨111⟩-direction, and a truncation of a octahedron as viewed along a ⟨100⟩-direction (right-bottom and right-top, respectively). By looking at this figure, the protuberances P1 and P2 may be recognized to correspond in shape with the cubo-octahedron and octahedron crystallographic forms, respectively. Furthermore, the observed micrometric protuberances, whatever is the cubic crystallographic habit they display, and the spatially coherent composite matrix were found to keep in common some important crystallographic directions. This finding is illustrated in Fig. 4b, where the protuberances P1 and P3 may be seen to be immersed within the matrix so that one of their respective ⟨110⟩-directions (light dashed-line in the figure) is parallel to the ⟨110⟩-direction of the crystal growth (heavy dashed-line in Fig. 4a). This finding opens the door to the possibility of using the studied spatially coherent composite growths as matrices for growing inside, oriented in the space along particular crystallographic directions, spatially coherent micrometric particles.

The observed surface steps were found to run parallel to each other, and also, to be sorted out by height, across the cleavage surface, so that they give place on this surface to a number of linear translational short-range-periodic surface-step patterns. Two of these patterns may be recognized to appear in Fig. 4a. One of these patterns is formed by surface steps with step heights of about 0.2 μm and a

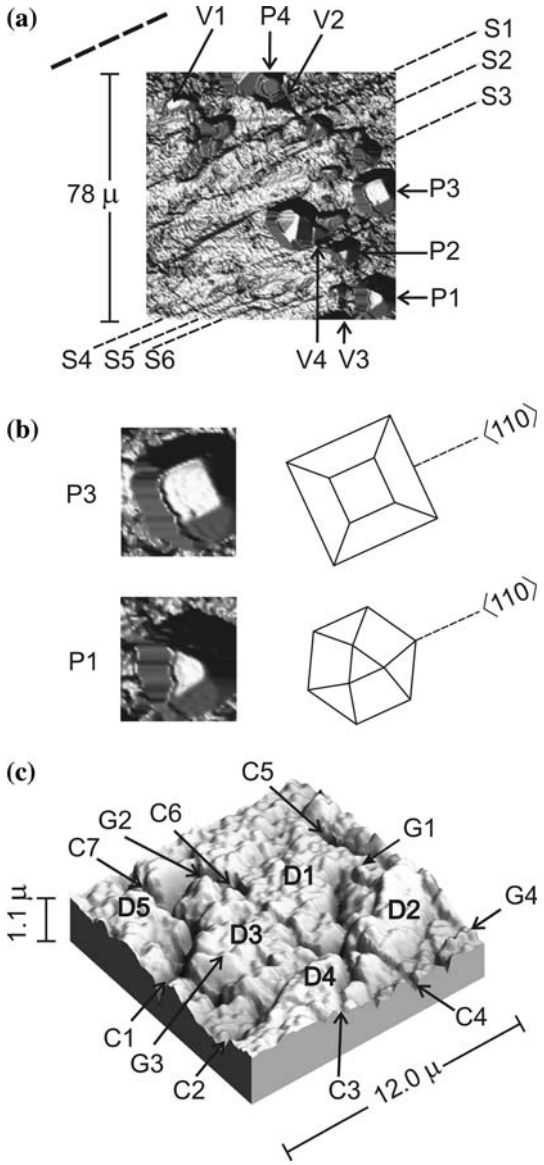

Fig. 4 (**a**) Typical AFM image of a freshly cleaved {100}-face obtained by exfoliating the crystal growth along a mechanically observed crystallographic ⟨110⟩-direction (heavy dashed-line at the top-left corner). Some micrometric protuberances (e.g., P1–P4) and cavities (e.g., V1–V4), as well as some straight surface steps (e.g., S1–S6) bearing wasted-away step edges, may be seen to be present on the inspected surface. Two short-range periodic surface-step patterns (one formed by S1–S3, and another by S4–S6) may be recognized. (**b**) Enlarged details showing the protuberances P1 (left-bottom) and P3 (left-top). Drafts of the cubo-octahedron and a truncation of the octahedron crystallographic forms, as viewed along the ⟨111⟩- and ⟨100⟩-directions, respectively, are also drawn (right-bottom and -top, respectively), for the sake of comparison. P1 and P3 may be seen to keep one of their respective ⟨110⟩-directions parallel to the cleavage ⟨110⟩-direction of the crystal growth. (**c**) High-resolution AFM image of a zone located between S2 and S3. Some irregular domains (e.g., D1–D5), each isolated from the others by deep canyons (e.g., C1–C7), containing numerous nanometric knolls (e.g., G1–G4) may be seen to form the inspected surface

translational period of about 3.0 μm (S1, S2, and S3 in the figure), while the other is formed by surface steps with step heights of about 0.9 μm and a translational period of about 10.2 μm (S4, S5, and S6 in the figure). In all the cases, the observed surface steps were found to be aligned to the exfoliation direction (heavy dashed-line in Fig. 4a), indicating that these steps are due (as discussed in section "On the structural origin of the observed surface steps") to the existence of a forest of screw dislocations within the studied composite.

In order to look for the structural origin of the observed lack of homogeneity in the mechanical response to cleavage of the composite under study, high-resolution AFM images were taken of surface-step free zones of freshly cleaved faces. One of these images, corresponding to the zone located between the surface steps S2 and S3 in Fig. 4a, is shown in Fig. 4c (an overall area roughness mean value of 5.4 ± 0.1 nm was measured for this zone). In this figure, the inspected surface may be seen to consist of a number of irregular domains (e.g., D1–D5) each isolated from the others by deep canyons (e.g., C1–C7). For these domains an individual average area of about 9 μm^2 was estimated, while the observed canyons were found to have depths in the range from 0.2 to 0.5 μm. The observed surface domains were found to be formed by numerous knolls (e.g., G1–G4 in Fig. 4c), with a measured surface density of 1.8 ± 0.1 knolls/μm^2 and an average height-profile full-width-at-half-maximum value of 0.054 ± 0.003 μm. The presence of these knolls suggests that the bulk of the spatially coherent composite under study is made of a mass of grains of nanometric size. These grains could be responsible for the observed inhomogeneous mechanical response to cleavage, and also (as discussed in section "On the origin of the observed lack of optical transparency") for the visual whitish appearance of the crystal growths.

Discussion

On the identity of phase B

In order to identify phase B as KI(34.36%):RbI(65.64%), the authors assumed previously that this phase was a binary phase, then, under this assumption, phase B was assigned to the solid-solution KI:RbI system on the basis, firstly, of the measured a_{0B}-value, and, secondly, of the measured I_{111}-value for this phase, and, finally, the relative concentrations of the KI- and RbI-type components in phase B were obtained by applying strictly the Vegard's rule. The authors could also have assumed that phase B was a ternary

phase, instead of a binary phase, by including the proposed binary KI:RbI composition, a certain amount of RbCl-, KBr-, RbBr-, or KCl-type components. However, from the salts corresponding to these alkali-halide components only RbBr satisfies the empirical 10%-unit-cell size difference criterion with both of the salts corresponding to the alkali-halide-type components of the proposed binary KI:RbI system, and, therefore, the composition of phase B as a ternary phase would be restricted to that of the KI:RbI:RbBr system. This ternary system is, under energetic grounds, less probable to form than the KI:RbI system since in the ternary case both cations and anions have to be exchanged.

On the identity of phase Q

Since no I^- ions were found to form phase of phase Q, no matter whether this phase is thought to exist as a binary, ternary, or quaternary solid-solution, only K^+-, Rb^+-, Cl^-, and Br^--ions are expected to form part of phase Q. Therefore, a general approach toward the knowledge of the chemical composition of phase Q may be done by, firstly, handling this phase as forming part of the quaternary KBr:RbCl:RbBr:KCl system, and, secondly, finding out the relative concentrations of the different alkali-halide-type components in this system. This approach will be followed here. Since X-ray diffraction experiments [26] carried out on the KBr:RbCl:RbBr:KCl system support the fact that this system satisfies a generalized Vegard's rule for quaternary solid-solutions, such generalized rule may be written for phase Q as follows,

$$wa_{0\mathrm{KBr}} + xa_{0\mathrm{RbCl}} + ya_{0\mathrm{RbBr}} + za_{0\mathrm{KCl}} = f_{\mathrm{Q}}a_{0\mathrm{Q}}, \quad (1)$$

where $a_{0\mathrm{KBr}}$, $a_{0\mathrm{RbCl}}$, $a_{0\mathrm{RbBr}}$, and $a_{0\mathrm{KCl}}$ are for the unit-cell sizes of the KBr, RbCl, RbBr, and KCl salts, respectively; w, x, y, and z are for the relative molar concentrations, in terms of the total amount of the mother-melt material, of the KBr-, RbCl-, RbBr-, and KCl-type components in the quaternary KBr:RbCl:RbBr:KCl solid-solution; and f_{Q} is for the mother-melt molar fraction that gave place to phase Q. This fraction is, by definition, given by the following ion-balance equation

$$f_{\mathrm{Q}} = w + x + y + z. \quad (2)$$

Since no I^- ions were found to form part of phase Q, all the I^- ions in the mother-melt must be inferred to be forming part of phase B. This inference, together with the fact that the anions forming phase B resulted to be only I^- ions, means that this phase is formed by a fraction of 1/3 of the total amount of the anion–cation pairs in the mother-melt, and, therefore, that phase Q is formed by a molar fraction of 2/3 of the full mother-melt material. Consequently,

$$f_{\mathrm{Q}} = 2/3. \quad (3)$$

Since the anions forming phase B are only I^- ions the total contents of the Cl^- and Br^- ions in the mother-melt (each equal to a fraction of 1/3 of the full mother-melt anion content) are constricted to form part of phase Q. Such constriction gives place to two other ion-balance equations, which are not independent from each other since they both represent only one ion-balance condition. One of these ion-balance equations (the one corresponding to the case of the Cl^- ions) is the following

$$x + z = 1/3. \quad (4)$$

In order to obtain another independent ion-balance equation, the relative molar concentrations found for the KI- and RbI-type components in phase B (0.3436 and 0.6564, respectively) may be conveniently expressed as fractions of the whole mother-melt material, obtaining 0.1145 ($\approx 0.3436 \times 1/3$) and 0.2188 ($\approx 0.6564 \times 1/3$), respectively. The first of these figures means that a fraction of 0.0522 ($\approx 1/6 - 0.1145$) of the amount of K^+-ions in the precursor KI salt is not forming part of the KI-type component of phase B, and, therefore, that this fraction of the K^+-ions in the precursor KI salt is forming part of the KBr- and KCl-type components of phase Q. Hence, the total amount of K^+-ions in phase Q must be given by the fraction of 0.0522 of the amount of K^+-ions in the precursor KI salt plus the whole amount of K^+-ions in the precursor KBr and KCl salts, i.e.,

$$w + z = 0.0522 + \frac{1}{6} + \frac{1}{6} = 0.3855. \quad (5)$$

For symmetry reasons, a fraction of about 0.0522 ($\approx 0.2188 - 1/6$) of the total amount of Rb^+-ions in the precursor RbCl and RbBr salts is forming part, in addition to the amount of the Rb^+-ions in the precursor RbI salt, of the RbI-type component of phase B, and, therefore, such additional Rb^+-ions in phase B must be absent in phase Q. However, the ion-balance equation corresponding to this last constriction is not independent from Eq. 5 since they both represent a unique ion-balance condition. A solution of the equation system consisting of Eqs. 1–5 is given, as can be demonstrated by direct substitution, by $w = 0.280$, $x = 0.218$, $y = 0.053$, and $z = 0.105$. Therefore, by expressing these values as relative concentrations of the alkali-halide-type components in phase Q, this phase may be represented by the quaternary KBr(42.7%):RbCl(33.2%):RbBr(8.1%)KCl(16.0%) solid-solution.

On the consequences of the observed crystallographic texture on the physical properties

Since the studied composite material resulted to be strongly textured this material is expected to inherit, from the component crystallites, the physical properties that are due

to the crystallite spatial-coherent nature, like the crystallite-lattice anisotropy-depending properties. In such a case, the inherited properties may be tailored as needed in the composite as a whole by tuning either the relative amounts of crystallites of the different component phases or the chemical composition of these phases or both. Further work is needed to verify the validity of this expectation.

On the origin of the observed lack of optical transparency

The as-grown crystal bulks of the novel material here reported have a whitish visual appearance instead of the transparent visual appearance that characterizes not only alkali-halide single-crystals and binary alkali-halide solid-solutions but also the ternary and quaternary alkali-halide solid-solutions that have been recently studied [24–26, 35]. The structural cause of this lack of optical transparency is probably associated to the structural cause of the observed lack of mechanical homogeneity in the material under study. High-resolution AFM images of freshly cleaved faces, showing that the inspected surfaces are formed by irregular domains with numerous knolls of nanometric size, suggested that the bulk of the spatially coherent composite under study is formed by a mass of nanometric individual grains. These grains are probably responsible for the observed inhomogeneous mechanical response to cleavage, while the borders of these grains, acting as scattering surfaces for light, are probably responsible for the whitish visual aspect of the material under study. This last proposition is not contrary to the known fact that impurities present in the precursor materials may contribute to the milky aspect of the crystal growth [36] by precipitating preferably along crystal dislocations and grain boundaries as the temperature diminishes toward room temperature during the cooling process. However, optical absorption as well as X-ray diffraction topography experiments should be carried out during the cooling process from freezing to room temperature in order to be able to detect any correlation existing between the optical absorption properties of the crystal growth and the thermal evolution of the grain boundaries in these growths.

On the structural origin of the observed surface steps

The finding that the observed surface steps appear on the inspected cleavage surfaces very nearly parallel to the exfoliation direction may be taken as an experimental evidence [37] of the fact that these steps are cleavage steps in origin. Since cleavage steps are commonly due [38] to the existence of a forest of screw dislocations which pierce the cleavage face, the presence of the observed surface steps indicates the existence of this type of dislocations in the material under study. This is the first experimental evidence, as far as the authors are aware, of the existence of screw dislocations in a spatially coherent alkali-halide composite.

Conclusions

Large crystal growths obtained from a melt that was previously prepared by mixing equal molar parts of KBr, RbCl, RbBr, KI, RbI, and KCl salts are formed by a novel strongly textured crystalline composite material. This material consists of an aggregation of crystallites of two different fcc-solid solutions identified as the binary KI(34.4%):RbI(65.6%) and the quaternary KBr(42.7%):RbCl(33.2%):RbBr(8.1%)KCl(16.0%) mixed phases, with respective unit-cell sizes of 7.247 ± 0.001 and 6.536 ± 0.005 Å. These phases form the composite in molar concentrations of 1/3 and 2/3, respectively. The crystallites are oriented in the space within the crystal growth so that their crystallographic ⟨100⟩-directions lie preferentially along the mechanically observed crystallographic ⟨100⟩-directions of the crystal-growth. Because of the observed crystallographic texture the studied growths may play an important role in the design and engineering of new spatially coherent mixed alkali-halide composites since they are expected to inherit, from the component crystallites, the physical properties that are due to the crystallite spatial-coherent nature like the crystallite-lattice anisotropy-depending properties. In the nanometric scale, the studied crystal growths consist of a mass of nanometric individual grains (with a measured area density of 1.8 ± 0.1 grains/μm^2 and an average size of 54 ± 3nm), which are probably responsible for both the observed inhomogeneous mechanical response to cleavage and the visual whitish appearance of the crystal growth. Freshly cleaved {100}-faces show surface steps which are identified as cleavage steps. The presence of these steps unveils, for the first time ever, the existence of screw dislocations in a spatially coherent mixed-alkali-halide composite. Some micrometric particles displaying cubic crystallographic habits are found to be immersed within bulk material so that they keep in common with the spatially coherent composite matrix some important crystallographic directions. This finding opens the door to the use of the studied crystal-growths as spatially coherent matrixes for growing inside, in a controlled manner, micrometric spatially coherent particles.

Acknowledgements The work is partially supported by the Dirección General de Asuntos del Personal Académico de la Universidad Nacional Autónoma de México (project PAPIIT-IN117506-3). The authors wish to thank Prof. Héctor Riveros Rotge and Mr. Ricardo Guerrero for growing the crystals and Mr. R. Unda-Angeles for doing the digital treatment of the images.

References

1. Bragg WH, Bragg WL (1913) Proc R Soc Lond Ser A 88:428. doi:10.1098/rspa.1913.0040
2. Bragg WL (1913) Proc R Soc Lond Ser A 89:248. doi:10.1098/rspa.1913.0083
3. Glocker R (1914) Phys Z 15:401
4. Glocker R (1915) Ann D Phys 47:377. doi:10.1002/andp.19153521104
5. Hull AW (1919) Trans Am Inst Electr Eng 38:1445
6. Davey WP (1921) Phys Rev 17:402
7. Wyckoff RWG (1921) J Washington Acad 11:429
8. Posnak E, Wyckoff RWG (1922) J Washington Acad 12:248
9. Vegard L, Schjelderup H (1917) Phys Z 18:93
10. Vegard L (1921) Phys Z 5:17. doi:10.1007/BF01349680
11. Kitaigorodsky AI (1984) Mixed crystals, chap 9. Springer-Verlag, Berlin, p 181
12. Sirdeshmukh DB, Srinivas K (1986) J Mater Sci 21:4117. doi:10.1007/BF01106517
13. Raynor GV (1958) Progress in metal physics, vol 1. Pergamon Press, London, p 61
14. Friedel J (1955) Philos Mag 46:514
15. "Powder Diffraction File" (International Centre for Diffraction Data, Pennsylvania, USA, 2001) data cards 36-1471, 6-0289, 8-0480, 4-0471, 6-0218 and 4-0587
16. Ohno T (1988) J Cryst Growth 91:576. doi:10.1016/0022–0248(88)90125-X
17. Smakula A, Maynard NC, Repucci A (1963) Phys Rev 130(1): 113
18. Priya M, Mahadevan CK, Physica B (2007) doi:10.1016/j.physb.2007.08.009
19. Shahaya Shajan X, Sivaraman K, Mahadevan C, Chandrasekharam D (1992) Cryst Res Technol 27:K79. doi:10.1002/crat.2170270433
20. Neelakanda Pillai N, Mahadevan CK (2007) Mater Manuf Processes 22:393. doi:10.1080/10426910701190972
21. Padma CM, Mahadevan CK (2007) Mater Manuf Processes 22:362. doi:10.1080/10426910701190808
22. Jayakumari K, Mahadevan CK (2005) J Phys Chem Solids 66:1705. doi:10.1016/j.jpcs.2005.07.008
23. Selvarajan G, Mahadevan CK (2006) J Mater Sci 8211. doi:10.1007/s10853-006-0999-2
24. Mijangos RR, Cordero-Borboa A, Camarillo E, Riveros H, Castaño VM (1998) Phys Lett A 245:123. doi:10.1016/S0375-9601(98)00370-3
25. Mijangos RR, Riveros H, Camarillo E, Guerrero R, Atondo M, Alvarez E, Rodriguez-Soria A (2000) Phys Stat Sol B 220:687. doi:10.1002/1521-3951(200007)220:1<687::AID-PSSB687>3.0.CO;2-U
26. Mijangos RR, Cordero-Borboa A, Alvarez E, Cervantes M (2001) Phys Lett A 282:195. doi:10.1016/S0375-9601(01)00184-0
27. Perumal S, Mahadevan CK (2005) Physica B 369:89. doi:10.1016/j.physb.2005.07.034
28. Corde-Roborboa AE, Mijangos RR, Schabes-Retchkiman PS (2006) J Mater Sci 41:7119. doi:10.1007/s10853-006-0932-8
29. Czochralski J (1918) Z Phys Chem 92:219
30. Cohen MU (1935) Rev Sci Instr 6:68. doi:10.1063/1.1751937
31. Cohen MU (1936) Zeit F Krist 94:288
32. Parrish W, Wilson AJC (1959) Precision measurement of lattice parameters of polycrystalline specimens. In International Tables for X-Ray Crystallography, vol II. Kinoch Press, Birminham, England, p 223
33. Cullity BD, Stock SR (2001) Elements of X-ray diffraction, 3rd edn. Prentice-Hall, Inc., NJ, p 141
34. Buerger MJ (1956) Elementary crystallography. Wiley, NY, p 114
35. Mijangos RR, Alvarez E, Perez-salas R, Duarte C (2004) Opt Mater 25:279. doi:10.1016/j.optmat.2003.07.004
36. Bunget I, Popescu M (1984) Physics of solid dielectrics. Materials Science Monographs, vol 19. Elsevier, Romania, p 153
37. Friedel J (1964) Dislocations. Pergamon Press Ltd, London, p 321
38. Fisher FC (1954) Acta Met 2:9. doi:10.1016/0001-6160(54)90087-5